

# Nickel-based metal-organic-frameworks as electrocatalysts for electrochemical oxidation of ammonia

Jun Zhai<sup>1</sup>, Xiaosi Ma<sup>1</sup>, Jujiao Zhao<sup>2,4</sup>, Yin Xiong<sup>3</sup>, Yanzong Tao<sup>3</sup>

<sup>1</sup>College of Environment and Ecology, Chongqing University, Chongqing 400045, P. R. China

<sup>2</sup>College of Environment and Resources, Chongqing Technology and Business University, Chongqing 400067, P.R. China

<sup>3</sup>Chongqing Baihan wastewater treatment Co., LTD, Chongqing 400000, P.R. China

<sup>4</sup>zhaojujiao@ctbu.edu.cn (Jujiao Zhao)

**Abstract.** Electrochemical oxidation of ammonia can produce hydrogen by splitting the ammonia molecules, not merely facilitating the elimination of ammonia but also augmenting sustainable hydrogen-based technological systems. However, the anode reaction is sluggish and the development of novel electrocatalysts is the major method to overcome this demerit. Herein, three kinds of Ni-based MOFs (Ni-BDC, Ni-BTC, and Ni-NH<sub>2</sub>-BDC) were prepared and used as electrocatalysts towards electrochemical oxidation of ammonia for the first time. At optimized working condition (0.5 V), Ni-NH<sub>2</sub>-BDC presents the response current density of 2.12 mA/cm<sup>2</sup> with the current efficiency of 92.6%, both of which are significantly higher than those of Ni-BDC and Ni-BTC, indicating the better performance of Ni-NH<sub>2</sub>-BDC. EIS tests and the measurement of conductivity revealed that the good performance of Ni-NH<sub>2</sub>-BDC could be attributed to the lower charge transfer resistance at the electrode/electrolyte interface and the significantly improved conductivity which is caused by the introduction of NH<sub>2</sub> groups. This work shed lights on the development of MOFs electrocatalysts for ammonia oxidation as well as other electrochemical reactions.

**Keywords:** Electrochemical oxidation of ammonia, Nickel-based MOFs, Wastewater treatment, Hydrogen production

## 1. Introduction

Ammonia is recognized as a principal water pollutant, with its concentrations in wastewater emanating from industries such as leather processing, coal chemical engineering, and aquaculture often exceeding 1000 mg/L [1]. Wastewater with high concentrations of ammonia typically exhibits poor biodegradability, challenging the effectiveness of biological treatment methods [2]. Concurrently, ammonia also serves as a potential energy-containing substance. The electrochemical oxidation of ammonia can produce hydrogen by splitting the ammonia molecules, not merely facilitating the elimination of ammonia but also augmenting sustainable hydrogen-based technological systems. The theoretical potential necessary for decomposing ammonia to generate hydrogen is just 0.06 V (*vs.* SHE) and the reaction could be seen as eq.1-3 [3,4]. However, the overpotential for ammonia oxidation at the

anode surface is substantial and the reaction rate is sluggish, curtailing the efficiency of ammonia removal and leading to elevated actual energy consumption [4].



The pursuit of novel electrocatalysts is pivotal in surmounting this challenge. Platinum (Pt), initially identified for its ability to oxidize ammonia at relatively low overpotentials, achieved the lowest overpotential at approximately 0.48 V, thus maintaining its status as the most effective ammonia oxidation electrocatalyst for an extended period<sup>5</sup>. However, the deactivation of Pt during the electrochemical oxidation of ammonia is very fast due to the too strong binding energy of N atoms on the Pt surface, significantly impeding the practical applications of Pt [5]. Moreover, the scarcity of noble metals like Pt poses an insurmountable challenge, underscoring the imperative need to develop abundant non-precious metal electrocatalysts [6].

Common anode materials in water treatment, such as boron-doped diamond [7] and lead dioxide (PbO<sub>2</sub>) [8], have been explored for electrocatalytic ammonia oxidation. Nevertheless, these materials necessitate an overpotential greater than 2 V to exhibit effective ammonia nitrogen removal capabilities. Presently, Ni-based materials among transition metals exhibit promising prospects, examples include Ni electrode [9], Ni/Ni(OH)<sub>2</sub> [10], and NiOOH/NF [11]. However, the electrocatalytic performance of these non-Pt materials in ammonia oxidation still falls short of requirements, intensifying the demand for economical and efficient novel anode catalysts for hydrogen production through ammonia oxidation.

Metal-Organic Frameworks (MOFs), comprising metal ions and organic ligands interconnected via coordination bonds, are porous crystalline materials [12]. Their compositional diversity, easily customizable morphology, tunable pore structures, and chemical modifiability render them highly versatile in fields such as gas storage, thermocatalysis, gas separation, and electrocatalysis [12]. Recently, MOFs have garnered extensive attention as direct electrocatalysts in electrochemical reactions such as oxygen evolution reaction [13] and CO<sub>2</sub> reduction [14]. Their distinctive porous architecture ensures effective dispersion and exposure of metal sites, favorable for catalytic reaction progression [14].

Crucially, the ligands in MOFs are not mere spectators; rather, they play a pivotal role in modulating the electrocatalytic activity [15]. This influence arises from their ability to alter the electronic environment of the metal centers, thus impacting the catalytic behavior. However, the application of MOF electrocatalysts in the electrochemical oxidation of ammonia remains nascent, with the field ripe for further exploration and discovery.

In this study, three distinct MOFs, namely Ni-BDC, Ni-NH<sub>2</sub>-BDC, and Ni-BTC, were synthesized employing benzene-1,4-dicarboxylic acid (BDC, 99%), 2-amino-1,4-benzene dicarboxylic acid (NH<sub>2</sub>-BDC), and 1,3,5-benzenetricarboxylic acid (BTC) as organic ligands, respectively. Their performance as electrocatalysts for electrochemical oxidation of ammonia was meticulously examined and the transformation of these materials during the electrochemical processes was revealed. The outcomes of this study promise to contribute to the development of innovative MOF-based electrocatalysts and propel the advancement in the wastewater treatment.

## 2. Methods and Materials

### 2.1. Chemicals and Materials

Benzene-1,4-dicarboxylic acid (BDC, 99%), 1,3,5-benzenetricarboxylic acid (BTC, 98%), 2-amino-1,4-benzene dicarboxylic acid (NH<sub>2</sub>-BDC, 98%), and Ni(II) nitrate hexahydrate (Ni(NO<sub>3</sub>)<sub>2</sub>·6H<sub>2</sub>O, 98%) were purchased from Macklin. Additional reagents, including N,N-dimethylformamide (DMF, 99%), sodium hydroxide (NaOH, >98%), and absolute ethanol (C<sub>2</sub>H<sub>5</sub>OH, 99.7%), were obtained from the Chongqing Chuandong Co. These chemicals were used as received without any further purification.

## 2.2. Preparation of samples

The Ni-BDC, Ni-NH<sub>2</sub>-BDC, and Ni-BTC were synthesized utilizing a straightforward solvothermal method. To prepare Ni-BDC, the 15 mL DMF solution containing 3 mmol BDC was mixed with a solution of 1 mmol Ni(NO<sub>3</sub>)<sub>2</sub>·6H<sub>2</sub>O in 30 mL DMF, followed by the gradual addition of 2.4 mmol NaOH dissolved in 30 mL water. This mixture was stirred continuously until fully blended. The resulting homogeneous solution was then transferred to a 100 mL Teflon-lined autoclave and heated at 120°C for 10 hours. After cooling to room temperature, the resultant precipitate was collected via centrifugation, sequentially washed with DMF, water, and ethanol, and subsequently dried at 40°C for 12 hours. The synthesis of Ni-NH<sub>2</sub>-BDC followed a similar procedure by replacing BDC to NH<sub>2</sub>-BDC.

For the synthesis of Ni-BTC, a mixture of 4 mmol BTC dissolved in 20 mL DMF and 20 mL absolute ethanol was prepared, and 1.33 mmol Ni(NO<sub>3</sub>)<sub>2</sub>·6H<sub>2</sub>O was dissolved in 20 mL water. The Ni(NO<sub>3</sub>)<sub>2</sub>·6H<sub>2</sub>O solution was gradually added to the BTC solution under continuous stirring until a homogenous mixture was obtained. This mixture was then transferred to a 100 mL Teflon-lined autoclave and heated at 150°C for 24 hours. Post-cooling, the precipitate was collected, washed, and dried using the similar method as described for the synthesis of Ni-BDC.

## 2.3. Characterization Methods

Morphological analysis was performed using a Talos F200S Transmission Electron Microscope (TEM) (Thermo Fisher Scientific CD Ltd, Czech Republic) with the accelerating voltage of 200 kV. Energy-Dispersive X-ray Spectroscopy (EDS) elemental mapping was also obtained by the same equipment. X-ray Diffraction (XRD) patterns were recorded on a Panalytical B.V. X-ray diffractometer (Holland), scanning from 5° to 90° with the scan rate of 2°/min. X-ray Photoelectron Spectroscopy (XPS) analysis was conducted on an ESCALAB 250Xi spectrometer (USA), using an Al K $\alpha$  X-ray source (1486.6 eV). The C-1s peak at 284.8 eV served as a reference for aligning all spectra. The conductivity of samples was measured by a YAOS FM100GH (China). The powder samples was pressed into bulk for the measurement with the pressure of 3 MPa.

## 2.4. Electrochemical Measurements

For electrode preparation, the synthesized sample was mixed with nafion solution and water to obtain the solution with 0.5% nafion. This mixture was then applied to a hydrophobic carbon cloth, covering an area of 1 cm<sup>2</sup>, with the loading mass of 1 mg/cm<sup>2</sup>. Electrochemical measurements were conducted using a standard three-electrode system. The prepared electrode served as the working electrode, complemented by a platinum sheet as the counter electrode and a saturated calomel electrode as the reference electrode. The electrolyte solution comprised a mixture of 0.5 M NaOH and 0.5 M ammonia. Before all the electrochemical measurements, the Cycle Voltammetry (CV) was conducted in 0.5 M NaOH to activate the sample until the current signal is stable. Electrochemical Impedance Spectroscopy (EIS) was performed in a frequency range from 0.01 Hz to 100 kHz to assess the charge transfer characteristics of the samples. Linear Sweep Voltammetry (LSV) was executed within a voltage range of 0-1 V at a scan rate of 10 mV/s.

# 3. Results and discussion

## 3.1. Characterization of catalysts

The crystalline structure was firstly evaluated by XRD. The XRD patterns of Ni-BDC, Ni-BTC, and Ni-NH<sub>2</sub>-BDC depicted in the provided Figure 1, offer critical insights into the phase purity and crystalline nature of the synthesized materials. The distinct diffraction peaks corresponding to each MOF signify successful synthesis and crystallization. For Ni-BDC, the peaks locating at 11.9°, 15.7°, and 24.8° was in accordance with the MOFs reported by Mahdi's group, confirmed the successful synthesis of Ni-BDC<sup>16</sup>. Similarly, Ni-BTC exhibits sharp and well-defined peaks, suggesting a high degree of crystallinity and confirming the formation of the desired MOF structure. Meanwhile, Ni-NH<sub>2</sub>-BDC

shows the distinct diffraction pattern which is similar to that of the reported MOFs with NH<sub>2</sub>-BDC as ligands [17]. Substantially, these XRD results conclusively affirm the successful synthesis of the Ni-based MOFs with their respective organic ligands.

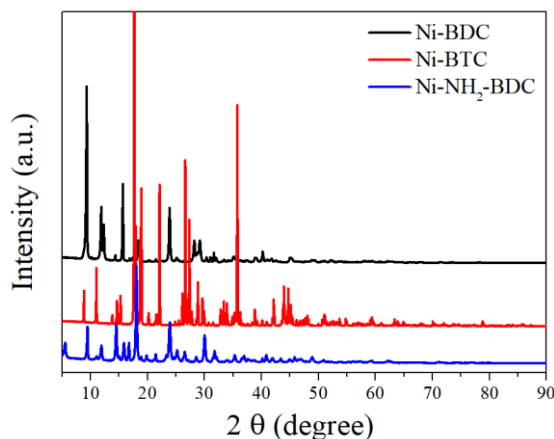


**Figure 1.** The XRD patterns of Ni-BDC, Ni-BTC, and Ni-NH<sub>2</sub>-BDC, respectively.

The TEM analysis was conducted on the samples to discern their morphological characteristics. As depicted in Figure 2, the TEM images reveal that both Ni-BDC and Ni-NH<sub>2</sub>-BDC samples exhibit a two-dimensional sheet-like structure with a parallelogram morphology. The defined edges and flat surfaces of the Ni-BDC and Ni-NH<sub>2</sub>-BDC samples could be observed. In contrast, the Ni-BTC sample displays a bulk morphology. The difference could be attributed to the different ligands which plays the important role in the morphology of MOFs. The results is also in agreement with the reported studies [13,16,17].

EDS elemental mapping provides further insight into the compositional homogeneity of the Ni-NH<sub>2</sub>-BDC. As shown in Figure 2d-f, the distribution of Ni is observed to be uniform, further indicating the successful synthesis of MOFs which is regarded to have the dispersed metal sites. The presence of N elements is identified by Figure 2f and the dispersion of N atoms is also uniform, providing the crucial evidence of the thorough incorporation of the NH<sub>2</sub> functional groups into the MOF structure. This uniformity is essential for facilitating consistent and efficient electrocatalytic reactions on the surface of electrocatalysts.

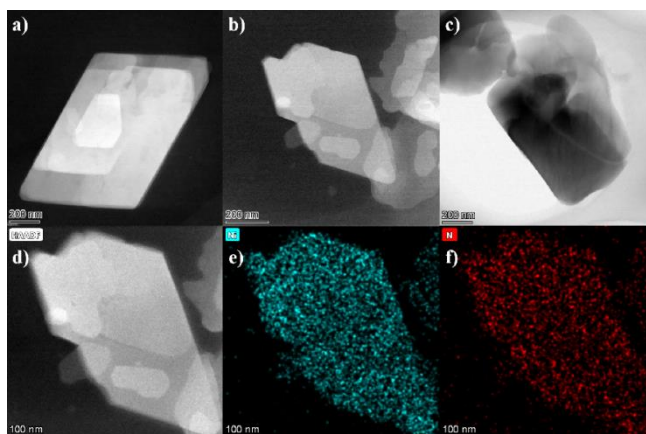


**Figure 2.** (a-c) The TEM images of Ni-BDC, Ni-BTC, and Ni-NH<sub>2</sub>-BDC, respectively; (d-f) The EDS images of Ni-NH<sub>2</sub>-BDC.

The chemical composition of the three MOF samples were investigated by XPS [18]. The XPS survey spectra (Figure 3) confirmed the presence of Ni, C, and O in all three samples. The Ni contents of Ni-BDC, Ni-NH<sub>2</sub>-BDC, and Ni-BDC are 4.94%, 3.83%, and 8.00%, respectively. The lowest Ni content of Ni-NH<sub>2</sub>-BDC might be attributed to the induction of NH<sub>2</sub> groups since it will lower the Ni/other elements ratio. Significantly, The peak corresponding to N atoms could be only seen in the spectrum of Ni-NH<sub>2</sub>-BDC, demonstrating the successful introduction of NH<sub>2</sub> groups. The N content Ni-NH<sub>2</sub>-BDC of is calculated to be 6.54%.

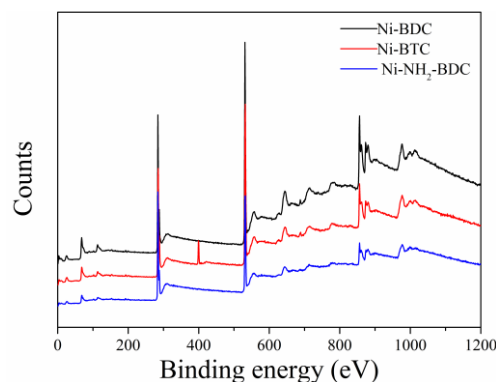


**Figure 3.** The XPS spectra of Ni-BDC, Ni-BTC, and Ni-NH<sub>2</sub>-BDC, respectively.

### 3.2. Electrochemical measurements of three MOFs samples

All the samples was activated by conducting the CV tests in 0.5M NaOH solution at first until the current is stable. For example, the CV curves of Ni-NH<sub>2</sub>-BDC for activation. The Linear Sweep Voltammetry (LSV) curves shown in Figure 4a illustrate the electrocatalytic activity of Ni-BDC, Ni-BTC, and Ni-NH<sub>2</sub>-BDC in a 0.5 M NaOH solution, with and without the addition of 0.5 M NH<sub>3</sub>. Upon introduction of ammonia into the electrolyte, a notable increase in current density is observed for all samples, which is indicative of ammonia oxidation. Notably, the Ni-NH<sub>2</sub>-BDC sample exhibits a significantly enhanced current density compared to the other two samples, both in the presence and absence of ammonia. This improvement suggests that the presence of the NH<sub>2</sub> functional group in the MOF structure facilitates the electrochemical process.

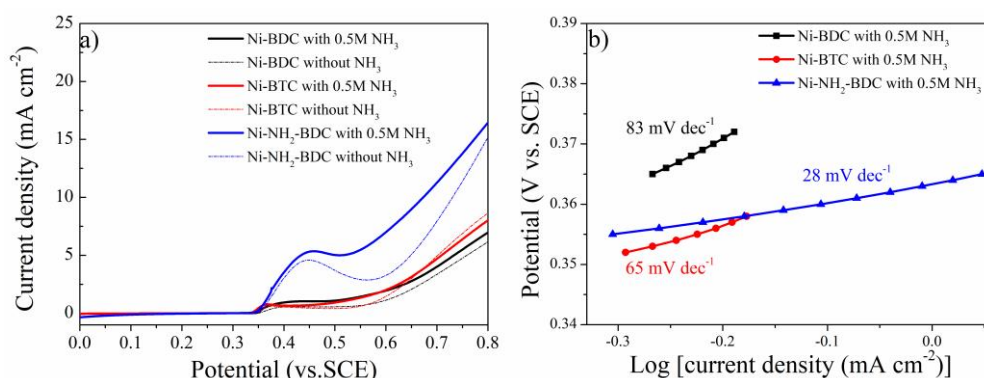


**Figure 4.** (a) The LSVs of Ni-BDC, Ni-BTC, and Ni-NH<sub>2</sub>-BDC, in 0.5 M NaOH with or without 0.5M NH<sub>3</sub>; (b) The calculated Tafel plots in 0.5 M NaOH with 0.5M NH<sub>3</sub>.

It could be noticed that the onset potential of Ni-NH<sub>2</sub>-BDC is 0.36 V, which is much similar to those of Ni-BDC and Ni-BTC. However, the current peak at around 0.45 V on the curve of Ni-NH<sub>2</sub>-BDC is much larger than those of Ni-BDC and Ni-BTC. According to the literature, this peak could be attributed to the oxidation of metals in the catalysts. Since all the three samples contains only Ni, these results might suggest the better electrochemical performance of Ni-NH<sub>2</sub>-BDC than others. Additionally, the

peak current density for Ni-NH<sub>2</sub>-BDC with ammonia at any working potential is the highest among the three samples. For example, at 0.8 V, the current density for Ni-NH<sub>2</sub>-BDC reaches approximately 16.93 mA/cm<sup>2</sup>, while the values for Ni-BDC and Ni-BTC are just 7.54 and 6.98 mA/cm<sup>2</sup>, respectively.

The Tafel slopes derived from the linear regions of the Tafel plot are indicative of the reaction mechanism and the rate-determining step of the electrochemical process [18]. As shown in Figure 4b, for the Ni-BDC, Ni-BTC, and Ni-NH<sub>2</sub>-BDC samples, the Tafel slopes are observed to be 83, 65, and 28 mV dec<sup>-1</sup>, respectively, when tested in the presence of NH<sub>3</sub>. The lower Tafel slope suggests a faster reaction kinetics, which is desirable in an electrocatalyst. Interestingly, despite the Tafel slope for Ni-BDC is larger than that for Ni-BTC, the Ni-NH<sub>2</sub>-BDC sample with NH<sub>2</sub>-group induced in BTC exhibits the lowest Tafel slope of 28 mV dec<sup>-1</sup>. These results indicate the more favorable electrochemical ammonia oxidation process with a faster electron transfer rate and a lower energy barrier of Ni-NH<sub>2</sub>-BDC compared to Ni-BDC and Ni-BTC. Since the Ni content of Ni-NH<sub>2</sub>-BDC is the lowest among the three samples and Ni was regarded as the active sites, the enhanced kinetics of Ni-NH<sub>2</sub>-BDC might be attributed to the improved electrical conductivity by the introduction of NH<sub>2</sub> functional groups. Overall, the Tafel analysis clearly demonstrates that Ni-NH<sub>2</sub>-BDC outperforms the other samples in terms of electrochemical ammonia oxidation with faster kinetics. These observations collectively indicate that Ni-NH<sub>2</sub>-BDC is a more active and efficient electrocatalyst for the oxidation of ammonia in alkaline media. Its modified structure, incorporating NH<sub>2</sub> groups, seems to facilitate better interaction with ammonia, leading to enhanced catalytic performance.

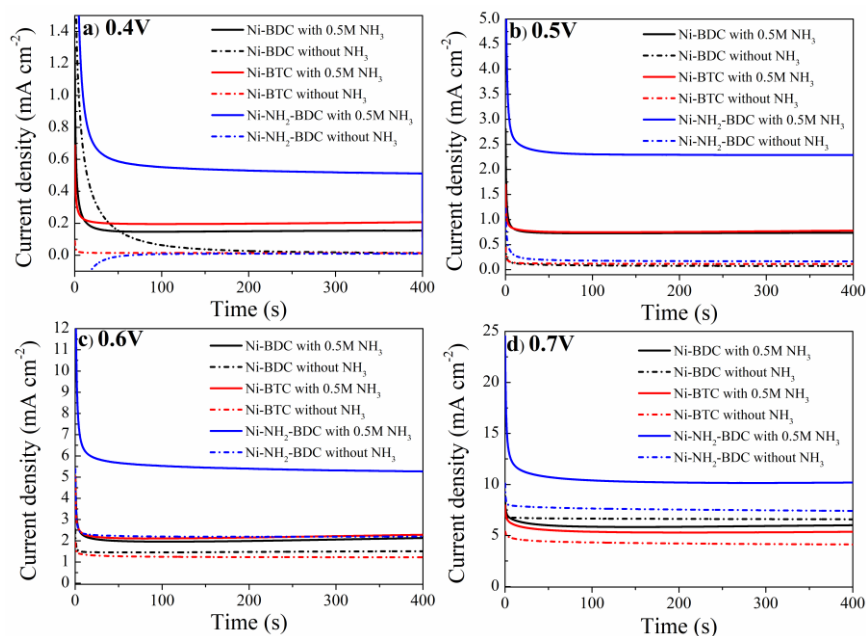


**Figure 5.** (a-d) Chronoamperogram of Ni-BDC, Ni-BTC, and Ni-NH<sub>2</sub>-BDC at 0.4 V, 0.5 V, 0.6 V, and 0.7 V, respectively, in 0.5 mol/L NaOH with 0.5 mol/L NH<sub>3</sub>.

To further reveal the electrochemical performance of the three samples, chronoamperometry tests were conducted to evaluate their electrocatalytic activities for ammonia oxidation at 0.4 V, 0.5 V, 0.6 V, and 0.7 V, respectively. As shown in Figure 5a, at 0.4 V, despite the three samples present similar current densities in pure 0.5 M NaOH, the Ni-NH<sub>2</sub>-BDC with 0.5 M NH<sub>3</sub> exhibits a much higher current density (0.51 mA/cm<sup>2</sup>) than those of Ni-BDC (0.15 mA/cm<sup>2</sup>) and Ni-BTC (0.21 mA/cm<sup>2</sup>) under the same condition, further indicating the better performance of Ni-NH<sub>2</sub>-BDC for electrochemical oxidation of ammonia. Increasing the potential to 0.5 V and 0.6 V further differentiates the performance of Ni-NH<sub>2</sub>-BDC. At these potentials, the maintained current density for the Ni-NH<sub>2</sub>-BDC with the presence of NH<sub>3</sub> remains notably higher than those for the other samples. Significantly, even without NH<sub>3</sub>, The Ni-NH<sub>2</sub>-

BDC also exhibits much higher current densities than Ni-BDC and Ni-BTC. At 0.7 V, the current densities of all samples increase, which could be due to the higher driving force for the electrochemical reaction. It could be noticed that the current density for Ni-NH<sub>2</sub>-BDC with the absence of NH<sub>3</sub> increases very much, which could be due to the oxygen evolution reaction [19]. However, Ni-NH<sub>2</sub>-BDC continues to outperform the other catalysts when excluding the influence of the oxygen evolution reaction. This suggests that the intrinsic electrochemical performance of Ni-NH<sub>2</sub>-BDC is much better than the two other samples and the Ni-NH<sub>2</sub>-BDC could maintain the best activity towards electrochemical oxidation of ammonia among these catalysts even at higher potentials.

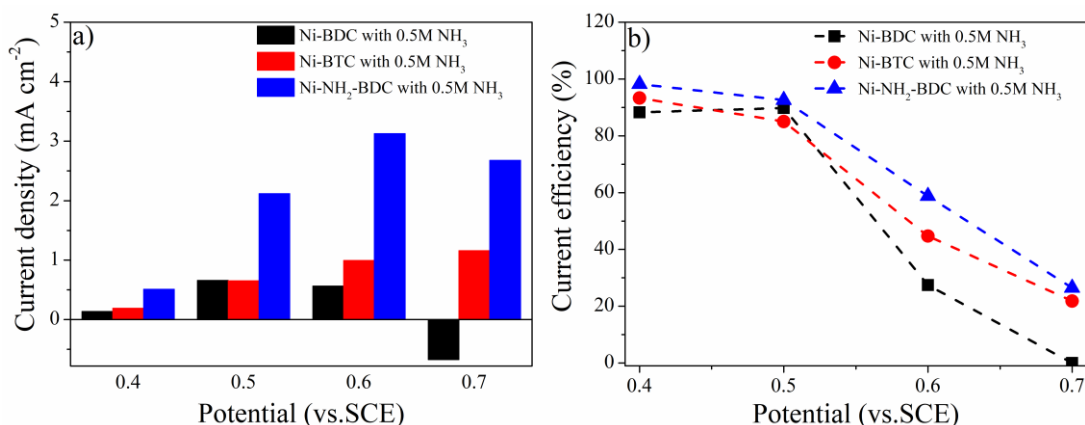


**Figure 6.** (a, b) The calculated response current towards ammonia and the current efficiency for ammonia oxidation.

To better illustrate the good performance of Ni-NH<sub>2</sub>-BDC, the response current and the current efficiency towards electrochemical oxidation of ammonia were calculated based on the results from Figure 5. As depicted in Figure 6, the current density towards ammonia of Ni-NH<sub>2</sub>-BDC is the highest at 0.4-0.7 V, indicating its superior initial electrocatalytic activity towards ammonia oxidation. It could also be noticed that the response current density increased when the working potential increased from 0.4 V to 0.6 V. The response current density at 0.5 V of Ni-NH<sub>2</sub>-BDC is 2.12 mA/cm<sup>2</sup>, which is 3.2 times higher than those of Ni-BDC (0.66 mA/cm<sup>2</sup>) and Ni-BTC (0.65 mA/cm<sup>2</sup>). The highest response current density of Ni-NH<sub>2</sub>-BDC is 3.13 mA/cm<sup>2</sup>, which could be obtained at 0.6 V. Further increasing the working potential to 0.7 V leads to the decreased current density of 2.68 mA/cm<sup>2</sup>. These results could be due to the enhanced oxygen evolution reaction at higher voltages.

The current efficiency of all the three samples at various voltages could be seen at Figure 6b. Significantly, compared to Ni-BDC and Ni-BTC, the Ni-NH<sub>2</sub>-BDC presents the highest current efficiency at any working potentials. At 0.5 V, the current efficiency of Ni-BDC, Ni-BTC, and Ni-NH<sub>2</sub>-BDC are 89.8%, 85.0%, and 92.6%, respectively. However, at 0.6 V the current efficiency of Ni-NH<sub>2</sub>-BDC decreased to 58.8%, but this value is still much higher than those of Ni-BDC (27.4%) and Ni-BTC (44.7%) under similar conditions. These results further demonstrate the better performance of Ni-NH<sub>2</sub>-BDC for the electrochemical oxidation of ammonia.

Based on the results shown above, the optimized working potential of Ni-NH<sub>2</sub>-BDC is suggested to be 0.5 V since the response current density at 0.4 V is too low meanwhile the current efficiency decreased significantly at 0.6 V.

### 3.3. Mechanism investigation

The electrochemical process on the surface of samples during the ammonia oxidation was investigated. Some studies reported that the MOFs will transform into amorphous structure when they are employed as anode in electrochemical reaction [13]. The XRD patterns of Ni-NH<sub>2</sub>-BDC loaded carbon cloth before and after the electrochemical oxidation of ammonia was depicted in Figure 7a. The peak at 18.9° was poly-tetrafluoroethylene, which belongs to the hydrophobic carbon cloth used as the substrate. It can be

seen that the electrode presents multiple crystal peaks belonging to Ni-NH<sub>2</sub>-BDC after the loading. However, after activation these crystal peaks all disappeared, indicating that during the electrochemical process the crystal structure of Ni-NH<sub>2</sub>-BDC has collapsed. Meanwhile, the XPS N1s of Ni-NH<sub>2</sub>-BDC after activation still could be observed (Figure 7b), indicating that the NH<sub>2</sub>-BDC ligands was not dissolved or decomposed. Based on these results, it could be concluded that the Ni-NH<sub>2</sub>-BDC transformed into amorphous state during the electrochemical process, in accordance with other studies [13].

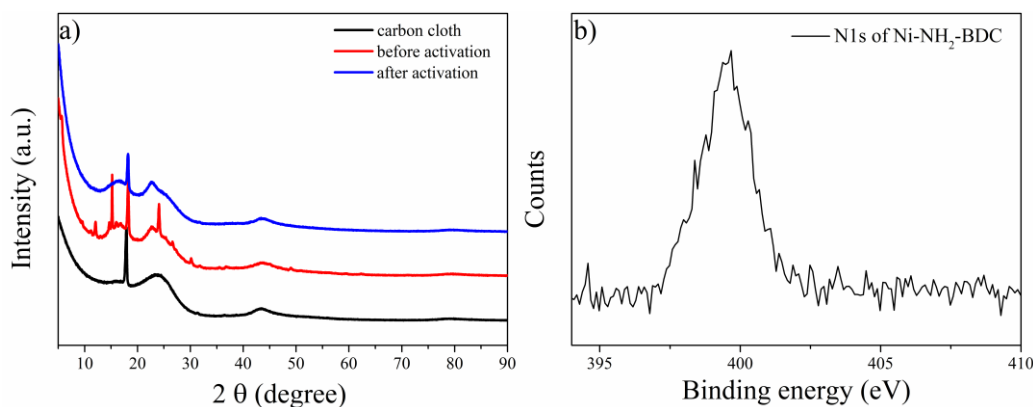


**Figure 7** (a) XRD patterns of carbon cloth, carbon cloth with Ni-NH<sub>2</sub>-BDC before and after activation; (b) The XPS N1s spectrum of Ni-NH<sub>2</sub>-BDC after activation.

To further reveal the origin of the good performance of Ni-NH<sub>2</sub>-BDC, EIS was measured and could be seen as Figure 8. The semicircle diameter in the high-frequency region correlates with the charge transfer resistance ( $R_{ct}$ ) at the electrode/electrolyte interface, which is a critical factor in determining the kinetics of the electrochemical reactions [17]. For Ni-NH<sub>2</sub>-BDC, the semicircle is significantly smaller than those for Ni-BDC and Ni-BTC, indicating that Ni-NH<sub>2</sub>-BDC possesses the lower charge transfer resistance. This result is consistent with the previous electrochemical data, which highlighted the superior performance of Ni-NH<sub>2</sub>-BDC. The lower  $R_{ct}$  could be attributed to the presence of the NH<sub>2</sub> functional groups in the Ni-NH<sub>2</sub>-BDC, which likely facilitate better charge delocalization and interaction with the electrolyte.

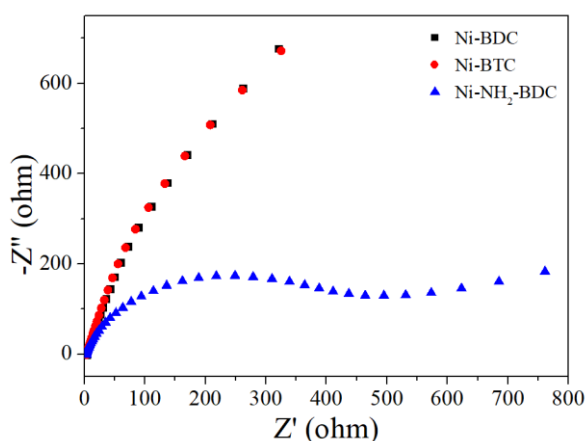


**Figure 8.** The EIS curves of Ni-BDC, Ni-BTC, and Ni-NH<sub>2</sub>-BDC, respectively.

Above results suggest that the Ni-NH<sub>2</sub>-BDC presents the better activity and lower charge transfer resistance. Also, it is revealed that the Ni-NH<sub>2</sub>-BDC contains the lowest content of Ni, which is generally regarded as the active sites. Based on these results, it is reasonable to speculate that the NH<sub>2</sub> groups

might enhance the conductivity of Ni-NH<sub>2</sub>-BDC, contributing to its good performance. To identify that, the conductivity of the three samples was tested and the conductivity values of Ni-BDC, Ni-BTC, and Ni-NH<sub>2</sub>-BDC are 0.04, 0.09, and 4.74  $\mu\text{s}/\text{m}$ . Ni-NH<sub>2</sub>-BDC exhibits the best conductivity and the value is over 40 times than those of Ni-BDC and Ni-BTC. Thus, this results demonstrate that the better performance of Ni-NH<sub>2</sub>-BDC might origin from its improved conductivity by the introduction of NH<sub>2</sub> groups.

#### 4. Conclusions

In this study, three kinds of Ni-based MOFs were prepared and used as electrocatalysts for electrochemical oxidation of ammonia. The optimized working potential is evaluated to be 0.5 V and Ni-NH<sub>2</sub>-BDC could exhibit the response current density of 2.12 mA/cm<sup>2</sup> with the current efficiency of 92.6%, both of which are significantly higher than those of Ni-BDC and Ni-BTC, indicating the better performance of Ni-NH<sub>2</sub>-BDC compared to Ni-BDC and Ni-BTC towards electrochemical oxidation of ammonia. EIS tests and the measurement of conductivity revealed that the better performance of Ni-NH<sub>2</sub>-BDC could be attributed to the lower charge transfer resistance at the electrode/electrolyte interface and the significantly improved conductivity which is caused by the introduction of NH<sub>2</sub> groups.

#### Conflicts of Interest

The authors declare no conflict of interest.

#### Acknowledgements

This work was supported by National Natural Science Foundation of China [grant number 22006005]; Natural Science Foundation of Chongqing [grant number CSTB2023NSCQ-MSX0700] and Chongqing Municipal Education Commission [grant number KJQN202300838].

#### References

- [1] Siddharth, K.; Chan, Y.; Wang, L.; Shao, M., Ammonia electro-oxidation reaction: Recent development in mechanistic understanding and electrocatalyst design. *Current Opinion in Electrochemistry* 2018, 9, 151-157.
- [2] Adli, N. M.; Zhang, H.; Mukherjee, S.; Wu, G., Review—Ammonia Oxidation Electrocatalysis for Hydrogen Generation and Fuel Cells. *Journal of The Electrochemical Society* 2018, 165, (15), J3130-J3147.
- [3] Kumar, S.; Magotra, V. K.; Jeon, H. C.; Kang, T. W.; Inamdar, A. I.; Aqueel, A. T.; Im, H.; Ahuja, R., Multifunctional ammonium fuel cell using compost as a novel electro-catalyst. *Journal of Power Sources* 2018, 402, 221-228.
- [4] Jeerh, G.; Zou, P.; Zhang, M.; Chen, S.; Humphreys, J.; Tao, S., Electrooxidation of ammonia on A-site deficient perovskite oxide La<sub>0.9</sub>Ni<sub>0.6</sub>Cu<sub>0.35</sub>Fe<sub>0.05</sub>O<sub>3- $\delta$</sub>  for wastewater treatment. *Separation and Purification Technology* 2022, 297, 121451.
- [5] Sacré, N.; Duca, M.; Garbarino, S.; Imbeault, R.; Wang, A.; Hadj Youssef, A.; Galipaud, J.; Hufnagel, G.; Ruediger, A.; Roué, L.; Guay, D., Tuning Pt–Ir Interactions for NH<sub>3</sub> Electrocatalysis. *ACS Catalysis* 2018, 8, (3), 2508-2518.
- [6] Hefnawy, M. A.; Fadlallah, S. A.; El-Sherif, R. M.; Medany, S. S., Synergistic effect of Cu-doped NiO for enhancing urea electrooxidation: Comparative electrochemical and DFT studies. *Journal of Alloys and Compounds* 2022, 896, 162857.
- [7] Michels, N.-L.; Kapałka, A.; Abd-El-Latif, A. A.; Baltruschat, H.; Comninellis, C., Enhanced ammonia oxidation on BDD induced by inhibition of oxygen evolution reaction. *Electrochemistry Communications* 2010, 12, (9), 1199-1202.
- [8] Shih, Y.-J.; Huang, Y.-H.; Huang, C. P., Oxidation of ammonia in dilute aqueous solutions over graphite-supported  $\alpha$ - and  $\beta$ -lead dioxide electrodes (PbO<sub>2</sub>@G). *Electrochimica Acta* 2017, 257, 444-454.

- [9] Li, Z.-F.; Wang, Y.; Botte, G. G., Revisiting the electrochemical oxidation of ammonia on carbon-supported metal nanoparticle catalysts. *Electrochimica Acta* 2017, 228, 351-360.
- [10] Shih, Y.-J.; Huang, Y.-H.; Huang, C. P., Electrocatalytic ammonia oxidation over a nickel foam electrode: Role of Ni(OH)<sub>2</sub>(s)-NiOOH(s) nanocatalysts. *Electrochimica Acta* 2018, 263, 261-271.
- [11] Zheng, W.; Li, Y.; Lee, L. Y. S., Insights into the transition metal ion-mediated electrooxidation of glucose in alkaline electrolyte. *Electrochimica Acta* 2019, 308, 9-19.
- [12] Yuan, S.; Feng, L.; Wang, K.; Pang, J.; Bosch, M.; Lollar, C.; Sun, Y.; Qin, J.; Yang, X.; Zhang, P.; Wang, Q.; Zou, L.; Zhang, Y.; Zhang, L.; Fang, Y.; Li, J.; Zhou, H. C., Stable Metal-Organic Frameworks: Design, Synthesis, and Applications. *Advanced materials* 2018, 30, (37), e1704303.
- [13] Sun, F.; Wang, G.; Ding, Y.; Wang, C.; Yuan, B.; Lin, Y., NiFe-Based Metal-Organic Framework Nanosheets Directly Supported on Nickel Foam Acting as Robust Electrodes for Electrochemical Oxygen Evolution Reaction. *Advanced Energy Materials* 2018, 8, (21), 1800584.
- [14] Nam, D. H.; Bushuyev, O. S.; Li, J.; De Luna, P.; Seifitokaldani, A.; Dinh, C. T.; Garcia de Arquer, F. P.; Wang, Y.; Liang, Z.; Proppe, A. H.; Tan, C. S.; Todorovic, P.; Shekhah, O.; Gabardo, C. M.; Jo, J. W.; Choi, J.; Choi, M. J.; Baek, S. W.; Kim, J.; Sinton, D.; Kelley, S. O.; Eddaoudi, M.; Sargent, E. H., Metal-Organic Frameworks Mediate Cu Coordination for Selective CO<sub>2</sub> Electroreduction. *Journal of the American Chemical Society* 2018, 140, (36), 11378-11386.
- [15] Mon, M.; Bruno, R.; Ferrando-Soria, J.; Armentano, D.; Pardo, E., Metal-organic framework technologies for water remediation: towards a sustainable ecosystem. *Journal of Materials Chemistry A* 2018, 6, (12), 4912-4947.
- [16] Salmanion, M.; Nandy, S.; Chae, K. H.; Najafpour, M. M., Further Insight into the Conversion of a Ni-Fe Metal-Organic Framework during Water-Oxidation Reaction. *Inorganic chemistry* 2022, 61, (12), 5112-5123.
- [17] Shahbazi Farahani, F.; Rahmanifar, M. S.; Noori, A.; El-Kady, M. F.; Hassani, N.; Neek-Amal, M.; Kaner, R. B.; Mousavi, M. F., Trilayer Metal-Organic Frameworks as Multifunctional Electrocatalysts for Energy Conversion and Storage Applications. *Journal of the American Chemical Society* 2022, 144, (8), 3411-3428.
- [18] Hao, Y.; Li, J.; Cao, X.; Meng, L.; Wu, J.; Yang, X.; Li, Y.; Liu, Z.; Gong, M., Origin of the Universal Potential-Dependent Organic Oxidation on Nickel Oxyhydroxide. *ACS Catalysis* 2023, 13, (5), 2916-2927.
- [19] Pieta, I. S.; Rathi, A.; Pieta, P.; Nowakowski, R.; Hołdyski, M.; Pisarek, M.; Kaminska, A.; Gawande, M. B.; Zboril, R., Electrocatalytic methanol oxidation over Cu, Ni and bimetallic Cu-Ni nanoparticles supported on graphitic carbon nitride. *Applied Catalysis B: Environmental* 2019, 244, 272-283.